Journal of Structural Biology xxx (xxxx) xxx–xxx

Contents lists available at ScienceDirect

Journal of Structural Biology

journal homepage: www.elsevier.com/locate/yjsbi

Structural analysis of phosphatidylinositol 4-kinase IIIβ (PI4KB) – 14-3-3 protein complex reveals internal flexibility and explains 14-3-3 mediated protection from degradation in vitro

Dominika Chalupska[a], Andrea Eisenreichova[a], Bartosz Różycki[b], Lenka Rezabkova[c], Jana Humpolickova[a], Martin Klima[a], Evzen Boura[a,*]

[a] Institute of Organic Chemistry and Biochemistry AS CR, v.v.i., Flemingovo nam. 2., 166 10 Prague 6, Czech Republic
[b] Institute of Physics, Polish Academy of Sciences, Al. Lotnikow 32/46, 02-668 Warsaw, Poland
[c] Laboratory of Biomolecular Research, Department of Biology and Chemistry, Paul Scherrer Institute, 5232, Villigen PSI, Switzerland

ARTICLE INFO

Keywords:
Lipid
Kinase
PI4KB
14-3-3 protein
Phosphatidylinositol
Small-angle X-ray scattering (SAXS)
GUV
Analytical ultracentrifugation
Structure
Proteolytical degradation

ABSTRACT

Phosphatidylinositol 4-kinase IIIβ (PI4KB) is responsible for the synthesis of the Golgi and trans-Golgi network (TGN) pool of phosphatidylinositol 4-phospahte (PI4P). PI4P is the defining lipid hallmark of Golgi and TGN and also serves as a signaling lipid and as a precursor for higher phosphoinositides. In addition, PI4KB is hijacked by many single stranded plus RNA (+RNA) viruses to generate PI4P-rich membranes that serve as viral replication organelles. Given the importance of this enzyme in cells, it has to be regulated. 14-3-3 proteins bind PI4KB upon its phosphorylation by protein kinase D, however, the structural basis of PI4KB recognition by 14-3-3 proteins is unknown. Here, we characterized the PI4KB:14-3-3 protein complex biophysically and structurally. We discovered that the PI4KB:14-3-3 protein complex is tight and is formed with 2:2 stoichiometry. Surprisingly, the enzymatic activity of PI4KB is not directly modulated by 14-3-3 proteins. However, 14-3-3 proteins protect PI4KB from proteolytic degradation in vitro. Our structural analysis revealed that the PI4KB:14-3-3 protein complex is flexible but mostly within the disordered regions connecting the 14-3-3 binding site of the PI4KB with the rest of the PI4KB enzyme. It also predicted no direct modulation of PI4KB enzymatic activity by 14-3-3 proteins and that 14-3-3 binding will not interfere with PI4KB recruitment to the membrane by the ACBD3 protein. In addition, the structural analysis explains the observed protection from degradation; it revealed that several disordered regions of PI4KB become protected from proteolytical degradation upon 14-3-3 binding. All the structural predictions were subsequently biochemically validated.

1. Introduction

Phosphatidylinositol 4-kinase IIIβ (PI4KB or PI4K IIIβ) produces, together with PI4K2A, the Golgi pool of phosphatidylinositol 4-phosphate (PI4P) (Boura and Nencka, 2015; Clayton et al., 2013). PI4P serves as a signaling molecule, and, additionally, as a precursor for higher phosphoinositides (Balla, 2013; Tan and Brill, 2014). PI4Ks and their product, PI4P, have also been implicated in human diseases such as cancer, Gaucher disease, several neural disorders and degeneration of spinal cord axons (Jovic et al., 2012; Jovic et al., 2014; Simons et al., 2009; Waugh, 2012, 2015). Additionally, PI4KB was identified as an essential host factor for several human viruses including poliovirus, hepatitis C virus, coxsackievirus B3, enterovirus 71, and Aichi virus and is, thus, considered a potential target for antiviral therapy (Altan-Bonnet and Balla, 2012; Berger et al., 2009; Dornan et al., 2016; Greninger et al., 2012; Sasaki et al., 2012; van der Schaar et al., 2013). Subsequently, highly specific inhibitors of PI4KB were developed (Mejdrova et al., 2015, 2017; Rutaganira et al., 2016; Sala et al., 2016) including fluorescent inhibitors (Humpolickova et al., 2017). Additionally, the crystal structures of PI4KB and other PI4K isozymes became available (Baumlova et al., 2014, 2016; Burke et al., 2014; Klima et al., 2015). Given the importance of this enzyme and its product, the PI4P lipid, in human physiology, the PI4KB enzyme should be tightly controlled within the cell. Indeed, several mechanisms were reported. PI4KB is a soluble cytoplasmic enzyme with no membrane binding properties yet it phosphorylates phosphatidylinositol embedded within the membrane. Therefore, it must be recruited to the target (Golgi) membrane. Recently, the Golgi resident protein ACBD3 was shown to be the major factor that recruits PI4KB to membranes and increases its enzymatic activity (Klima et al., 2017, 2016; McPhail et al.,

* Corresponding author.
E-mail address: boura@uochb.cas.cz (E. Boura).

http://dx.doi.org/10.1016/j.jsb.2017.08.006
Received 21 July 2017; Received in revised form 26 August 2017; Accepted 28 August 2017

2017). Another protein that has been reported to control the PI4KB enzymatic activity in the cell is the 14-3-3 protein (Hausser et al., 2005, 2006).

14-3-3 proteins are a highly conserved family of acidic regulators present in every eukaryotic organism from yeast to humans that have been reported to play a role in many diverse cellular processes ranging from signal transduction to carcinogenesis and apoptosis (Aghazadeh and Papadopoulos, 2016; Morrison, 2009). 14-3-3 proteins act in multiple diverse pathways because they regulate more than 300 binding partners that function in many cellular processes (de Boer et al., 2013; Obsilova et al., 2008a; Uhart and Bustos, 2014). 14-3-3 proteins recognize their binding partners upon phosphorylation of a specific serine or threonine residue although several binding partners that do not need to be phosphorylated have been described as well (Obsilova et al., 2014). Upon binding, they induce a specific molecular switch in their binding partners that can modulate their enzymatic activity (both up or down) (Ganguly et al., 2001; Lambeck et al., 2012), induce a conformational change (Rezabkova et al., 2011; Rezabkova et al., 2010), protect from dephosphorylation (Dent et al., 1995; Kacirova et al., 2015; Thorson et al., 1998) or change their subcellular localization as was reported for the FOXO4 transcription factor (Boura et al., 2010; Obsilova et al., 2005). PI4KB enzyme can be phosphorylated by protein kinase D (PKD) (Hausser et al., 2005) which was reported to protect PI4KB from dephosphorylation *in vivo* leading to increased PI4P production (Hausser et al., 2006). Here, we report on the structural basis for PI4KB regulation by 14-3-3 proteins. Surprisingly, we show that 14-3-3 does not directly increase the PI4KB enzymatic activity, however, we confer that it does protect the kinase from enzymatic degradation *in vitro* and that binding to 14-3-3 does not interfere with PI4KB membrane recruitment by ACBD3 protein.

2. Results and discussion

2.1. Biophysical characterization of PI4KB:14-3-3 protein complex

The interaction of PI4KB with 14-3-3 in a phosphorylation dependent manner is well documented in living cells (Hausser et al., 2005, 2006) and also the structure of yeast 14-3-3 protein Bmh1 with PI4KB derived phosphopeptide was solved recently (Eisenreichova et al., 2016). However, the PI4KB:14-3-3 protein complex formation was never shown *in vitro*. We used purified recombinant PI4KB (phosphorylated and non-phosphorylated) and 14-3-3ζ to characterize the PI4KB:14-3-3 protein complex *in vitro*. First we performed pull-down experiments and, as expected, only phosphorylated PI4KB was able to pull down 14-3-3 (Fig. 1A).

Next, we investigated the PI4KB:14-3-3 protein complex using analytical ultracentrifugation (AUC). Sedimentation velocity (SV) measurements revealed that PI4KB alone can dimerize with an apparent dissociation constant of 3 μM (Fig. 1B). Two peaks with weight average sedimentation coefficients (sw) of 4.3 S and 5.4 S corresponding to the monomer and dimer can be observed in the distribution. The dimerization is not affected by phosphorylation (Fig. 1C). As expected, continuous distribution of sedimentation coefficients – c(S) – of 14-3-3 protein showed a single peak with a sw of 3.6 S, which corresponds to a Mw of 56 kDa and is consistent with a dimeric-fold of the 14-3-3 protein family (Fig. 1D). Consistent with the pull-down experiments, non-phosphorylated PI4KB showed no significant interaction with 14-3-3, whereas phosphorylated PI4KB formed a stable complex with 14-3-3 (Fig. 1D). Analysis of SV data revealed that the binding stoichiometry of PI4KB:14-3-3 complex is preferentially 2:2 (dimeric 14-3-3 protein binds two molecules of PI4K). However, experiments with excess of 14-3-3 protein showed that the complex with 2:1 stoichiometry (dimeric 14-3-3 protein binds one molecules of PI4K) can also be formed (Fig. 1E). Although AUC estimates of molecular weights from complex protein mixtures are rather inaccurate because only an average friction coefficient is obtained during fitting in this case the theoretical and AUC estimated Mw correspond nicely (Fig. 1F).

Once the stoichiometry was known, we used microscale thermophoresis (MST) to determine the dissociation constant (K_d) of the PI4KB:14-3-3ζ protein complex. The capillaries were loaded with a mixture of the recombinant GFP-14-3-3ζ protein (100 nM) and phosphorylated or non-phosphorylated PI4KB kinase (a concentration range from 4 nM to 36 μM). The samples were excited with the 488 nm laser and the changes in thermophoresis were analyzed using the Monolith NT Analysis Software with the 1:1 stoichiometry model as suggested by AUC experiments yielding the apparent Kd of 175 ± 14 nM for the phosphorylated PI4KB while no interaction was observed for the non-phosphorylated PI4KB (Fig. 1G).

2.2. Structural characterization of PI4KB:14-3-3 protein complex

Crystallization trials using both full length and significantly truncated variants of PI4KB and 14-3-3 proteins have failed. We speculated that intrinsic flexibility and disorder of PI4KB could be the reason for the failed crystallization trials. The method of choice for analysis of large, flexible protein complexes is small angle X-ray scattering (SAXS) (Rozycki and Boura, 2014). Recently we co-developed the ensemble refinement of SAXS (EROS) method that is designed for structural characterization of flexible multi-protein complexes (Boura et al., 2011; Boura et al., 2012b; Rozycki et al., 2011) such as the membrane bending ESCRT system (Boura and Hurley, 2012; Rozycki et al., 2012). The EROS method requires structural (usually crystallographically- or NMR-derived) restrains, usually individual domains or subunits that are treated as rigid bodies. The crystal structures of PI4KB and 14-3-3 proteins are known (Burke et al., 2014; Liu et al., 1995). However, the details of 14-3-3 binding to the PI4KB phosphoserine 294 were not described before. In principle, homology modeling based on the known structure of Bmh1 (a yeast 14-3-3 homolog) with PI4KB-derived phosphopeptide (Eisenreichova et al., 2016) could be used. However, to be more accurate, we sought to solve the crystal structure of human 14-3-3ζ in complex with the PI4KB-derived phosphopeptide.

We mixed 14-3-3ζ with PI4KB-derived phosphopeptide (289-LKRTApSNPKV-298) and obtained crystals that diffracted to 2.1 Å resolution. The structure was solved by molecular replacement and refined to R_{work} = 18.79% and R_{free} = 23.11% as summarized in Table 1. The structure revealed the usual 14-3-3-fold – a dimer formed from two α-helical monomers (Fig. 2A). Each monomer is composed of nine α-helices that form a central phosphopeptide binding groove within each monomer. The density for the phosphopeptide was clearly visible upon molecular replacement. Compared to the previously solved structure of yeast 14-3-3 protein with PI4KB peptide (Eisenreichova et al., 2016) two additional residues (R291 and K290) were visible. However, we could not trace the first and last amino acid of the peptide (L289 and V298) suggesting that these two residues are already disordered. We conclude that they are part of the flexible linker that connects phosphoserine 294 (pS294) to the rest of the PI4KB. We also note that the segment 290-KRTApSNPK-297 that we could trace is missing (disordered or deleted) in all previous crystal structures of PI4KB (Burke et al., 2014; Fowler et al., 2016; Mejdrova et al., 2015, 2017). The PI4KB phosphopeptide is held in the 14-3-3 central binding groove by a series of hydrogen bonds. The phosphate group of $pS294^{PI4KB}$ interacts with sidechains of $R56^{14\text{-}3\text{-}3}$, $R127^{14\text{-}3\text{-}3}$, and $Y128^{14\text{-}3\text{-}3}$ while $K49^{14\text{-}3\text{-}3}$, $N173^{14\text{-}3\text{-}3}$, $N224^{14\text{-}3\text{-}3}$, and $W228^{14\text{-}3\text{-}3}$ form hydrogen bonds with the backbone of the PI4KB peptide (Fig. 2B). Importantly, the sidechain of residue $T292^{PI4KB}$ makes no contacts with the 14-3-3 protein suggesting that its mutation will not influence PI4KB binding to 14-3-3 protein.

With all the prerequisites in place, we utilized SAXS in combination with molecular dynamics simulations to reveal the structure of the PI4KB:14-3-3 protein complex. We collected the SAXS data using equimolar mixtures of phosphorylated PI4KB and 14-3-3ζ at different concentrations, which were at least three orders of magnitude larger than the dissociation constant of the PI4KB:14-3-3ζ complex. The

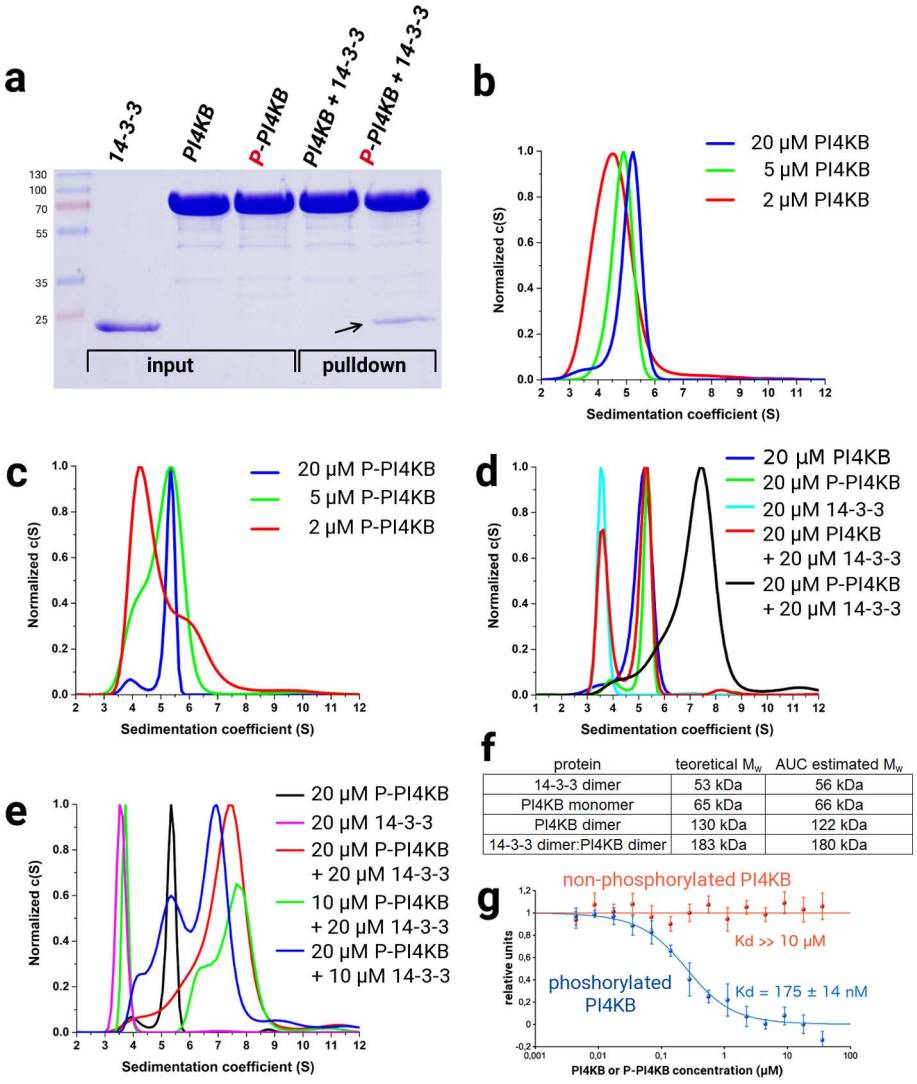

Fig. 1. Analysis of PI4KB binding to 14-3-3. A) Pull-down experiments were performed using purified recombinant proteins. Fusion proteins His_{8x}-SUMO-PI4KB or phosphorylated His_{8x}-SUMO-PI4KB were immobilized on Ni-NTA agarose beads and incubated with untagged 14-3-3. Eluted protein samples were analyzed by SDS-PAGE. Lines 1,2 and 3 represent 14-3-3, His_{8x}-SUMO-PI4KB, and phosphorylated His_{8x}-SUMO-PI4KB proteins used as the input in the experiment. Lines 4 and 5 represent the pull-down experiment, in line 4 the non-phosphorylated His_{8x}-SUMO-PI4KB was used as bait, in line 5 the phosphorylated His_{8x}-SUMO-PI4KB was used as bait for the 14-3-3. B-E) SV-AUC analysis of PI4K and its interaction with 14-3-3 protein. B, C) c(S) distribution profiles of PI4KB (B) and phosphorylated PI4KB (P-PI4KB) (C) showing the dimerization of the protein. D) c (S) distribution profiles showing that the phosphorylation of PI4KB is necessary for interaction with the 14-3-3 protein. E) c(S) distribution profiles of different ratios between PI4K-P and 14-3-3 revealing that P-PI4KB:14-3-3 complex is preferentially formed with 2:2 stoichiometry. F) Table comparing the theoretical and AUC estimated molecular weights. G) MST analysis of the interaction of the phosphorylated PI4KB (blue line) and non-phosphorylated PI4KB (orange line) kinase and the GFP-14-3-3 fusion protein. Change in relative thermophoresis and the concomitant fitting curve are shown. Data are presented as mean values ± standard errors of the means based on three independent experiments.

Table 1
Statistics of crystallographic data collection and refinement.

Data collection	
Crystal	14-3-3ζ with PI4KB peptide
X-ray source	BESSY ID 14.1
Wavelength, Å	0.97625
Space group	$P2_12_12_1$
Cell dimension	a = 71.82 Å, b = 83.55 Å, c = 111.54 Å
Resolution, Å	48.94 – 2.08 (2.154 – 2.08)
No. of unique reflections	41025 (4034)
I/σ (I)	21.76 (3.38)
R_{merge}	9.3 (98.5)
Data completeness,%	99.99 (100.00)
Multiplicity	15.9 (16.2)
$CC_{1/2}$	0.998 (0.82)
Refinement	
R_{work},%	18.79 (26.60)
R_{free},%	23.11 (31.02)
rms bond angle deviation, °	0.008
rms bond angle deviation, Å	0.95
Ramachandran (outliers/favored)	0%/99%

Numbers in parentheses refer to the highest resolution shell.

corresponding SAXS data sets (Table 2) overlay after rescaling (Fig. 3A), indicating no protein aggregation in the samples. The Guinier plot (inset in Fig. 3A) shows that the radius of gyration of the PI4KB:14-3-3ζ complex is 54 Å.

Next, we performed a series of molecular simulations of the PI4KB:14-3-3ζ protein complex with 2:2 stoichiometry and compared the simulation results with the experimental SAXS data. We found that many simulation structures were consistent with the SAXS data (Fig. 3B and C). We thus selected 'top 20' structures that individually fit the SAXS data best (χ^2 = 1.5–1.7) and sorted them into three groups based on the mutual similarity in the location of the two PI4KB monomers. Fig. 3C shows three exemplary structures that represent these three groups, and Fig. 3B compares their scattering intensity profiles with the experimental SAXS data. These three structures have a radius of gyration of 54 Å. Their maximum extension is in the range of 180–190 Å. Their characteristic dimensions, R_g and D_{max}, appear to be typical within the pool of simulation structures.

Overall, the PI4KB:14-3-3 models that fit the SAXS data are mutually similar (Fig. 3C). Interestingly, in all of these models, the active site of PI4KB is not occluded by 14-3-3 and presented away from the PI4KB:14-3-3 complex. This observation has far-reaching implications, as we discuss in the subsequent paragraphs. The characteristic hyperbolic feature of the Kratky plot (Fig. 3B) at high q-values (q > 0.25/Å) (Rozycki and Boura, 2014) indicates flexibility of the PI4KB:14-3-3 complex. To gain insights into the source of the molecular flexibility, we performed an EROS analysis which is devised to determine a minimum ensemble of simulation structures that fits the experimental SAXS data (Boura et al., 2011; Boura et al., 2012b). However, this

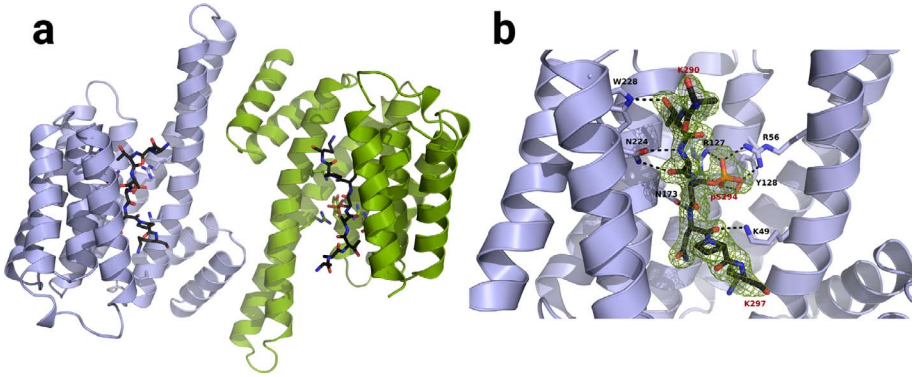

Fig. 2. The crystal structure of 14-3-3ζ with a PI4KB derived phosphopeptide. A) The overall fold. 14-3-3ζ is in cartoon representation and colored in blue and green, the phosphopeptide is in stick representation. B) Detailed view of the 14-3-3ζ binding groove with PI4KB phosphopeptide. An unbiased F_o-F_c omit map contoured at 3σ is shown in green.

Table 2
Characterization of the SAXS data.

Protein concentration	c = 1.17 mg/ml	c = 2.72 mg/ml	c = 3.97 mg/ml
Gunier analysis			
q-range	0.005–0.025 (1/Å) $0.26 \leq q R_g \leq 1.29$ 77 data points	0.005–0.024 (1/Å) $0.27 \leq q R_g \leq 1.3$ 73 data points	0.005–0.023 (1/Å) $0.28 \leq q R_g \leq 1.29$ 70 data points
R_g	51.4 Å	53.8 Å	55.6 Å
$I(0)$	85390	218110	482620
P(r) function			
q-range	0.005–0.48 (1/Å) 1808 data points		
D_{max}	180 Å	180 Å	180 Å
R_g	53.1 Å	54.9 Å	55.9 Å
$I(0)$	85810	218100	479900
Porod Volume	286040 Å^3	315880 Å^3	338550 Å^3

approach did not lead to any significant improvement of the fit quality, and resulted in decreasing χ2 from about 1.5 to only about 1.3. Moreover, the resulting models were found to be rather similar to those depicted in Fig. 3C. These results indicate that the 2:2 PI4KB:14-3-3 protein complex in solution does not exhibit excessive conformational variability, except for the disordered segments connecting the phosphopeptide with the PI4KB domain.

The main aim of this study was to elucidate the molecular architecture of PI4KB:14-3-3 protein complex. We failed to obtain crystals despite immense efforts presumably because of the intrinsic flexibility of the PI4KB:14-3-3 complex. SAXS is increasingly used as the method of choice for the analysis of intrinsically disordered or flexible proteins. We used SAXS in combination with molecular dynamics simulations to obtain structural insight into the assembly of PI4KB:14-3-3 protein complex. Many of the PI4KB:14-3-3 structures generated in the simulations were found to fit the SAXS data very well. These structures are similar overall – in terms of their dimensions (R_g and D_{max}) as well as the positioning of the two PI4KB monomers with respect to the 14-3-3 dimer – but differ in the relative orientation of PI4KB subunits with respect to the 14-3-3 protein core (Fig. 3C). The structural explanation

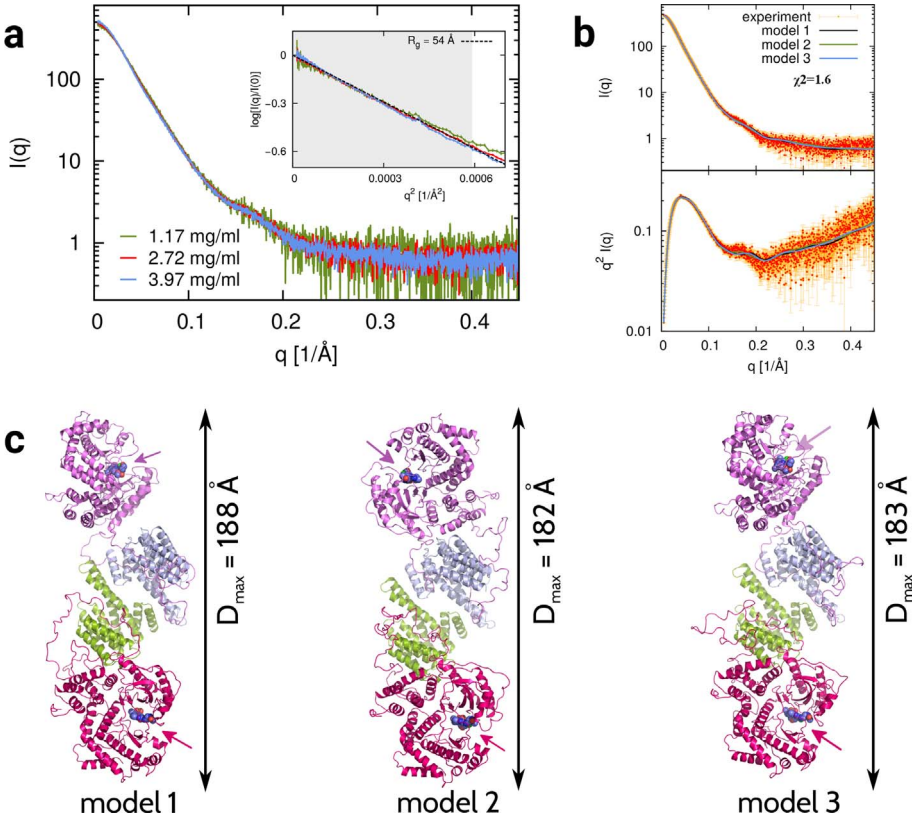

Fig. 3. SAXS analysis of PI4KB:14-3-3 protein complex. A) Experimental SAXS intensity as a function of momentum transfer, q, obtained at three different protein concentrations (1.17 mg/ml – green, 2.72 mg/ml – red, 3.97 mg/ml – blue). Note that the logarithmic scale is used on the vertical axis. Inset: The region $qR_g < 1.3$ where the Guinier approximation is valid for a globular protein is shaded gray. The dashed line indicates the best fit of the Guinier approximation, which leads to R_g = 54 Å. B) Experimental (c = 2.72 mg/ml – red) and theoretical (model 1 – black, model 2 – green, model 3 – blue) scattering data shown as $I(q)$ vs. q (top) and $q^2I(q)$ vs. q (Kratky plot; bottom). Any of the three models fits the experimental SAXS data with χ2 = 1.6. C) Three representative models of the 2:2 PI4KB:14-3-3 complex (PI4KB – magenta and purple, 14-3-3 – green and blue) that fit the experimental SAXS data. Their scattering profiles are shown in panel B in black, green and blue, respectively. The active site in the PI4KB enzyme is highlighted by a modeled inhibitor (magenta and purple arrows).

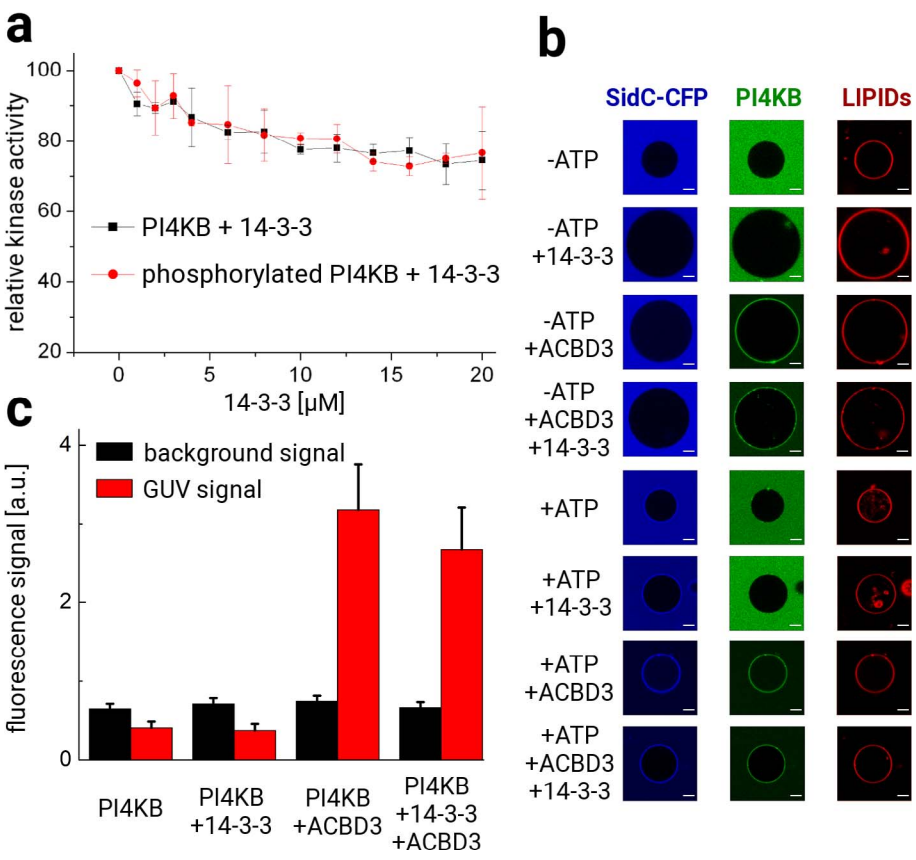

Fig. 4. Lipid kinase activity and recruitment assay. A) The lipid kinase activity was determined using ADP-GloTM Kinase Assay (Promega). The activity of phosphorylated and non-phosphorylated PI4KB in the absence of 14-3-3ζ was set to 100%. Presence of 14-3-3 in the concentrations ranging from 1 to 20 μM had slightly inhibiting effect on lipid kinase activity of both PI4KB or phosphorylated PI4KB. Shown are the mean values calculated from three independent experiments with the associated errors (s.d.). B) Membrane recruitment assay. GUVs containing ATTO647-DOPE as a membrane marker (red) were mixed with 600 nM P-PI4KB labeled by Alexa488 (green). PI4P production was visualized by the PI4P biosensor CFP-SidC (blue) that was added at 250 nM concentration. The reaction was carried out with or without ATP, ACBD3 and 14-3-3 as indicated. The scale bar is 6 μm. C) Quantification of membrane recruitment of PI4KB – mean fluorescence signal of Alexa488-labeled PI4KB on the surface (red columns) of GUVs and in the surrounding space (black columns) in the presence/absence of 14-3-3 and ACBD3. The error bar stands for the standard error of the mean.

is rather simple. The long, disordered linkers within PI4KB that contain the 14-3-3 binding site allow for multiple conformations of the PI4KB monomers respective to the 14-3-3 proteins. However, steric hindrance prevents too compact structures of PI4KB:14-3-3 protein complex at the preferred 2:2 stoichiometry. Notably, the PI4KB active site is well accessible in each of our model structures (colored arrows in Fig. 3C). Actually, our structural analysis predicts no effect of 14-3-3 binding on the activity of PI4KB. To verify our structural results, we measured PI4KB lipid kinase activity with and without 14-3-3. We did not observe any activation of the PI4KB kinase; however, we observed a very small decrease in its lipid kinase activity, albeit with poor statistical significance. Importantly, the enzymatic activity of the non-phosphorylated PI4KB that was used as a control also slightly decreased suggesting non-specific interference of 14-3-3 proteins with the assay used (Fig. 4A).

Our structural analysis also predicted that membrane recruitment of PI4KB by the ACBD3 protein would be unaffected by the 14-3-3 protein binding because the 14-3-3 binding site is distant from the disordered PI4KB N-terminus that binds ACBD3 (Klima et al., 2016). To further verify our structural model, we tested the membrane recruitment of PI4KB by membrane tethered ACBD3 in the biomimetic giant unilamellar vesicle (GUV) system. As expected, phosphorylated PI4KB was recruited regardless of the presence of 14-3-3 (Fig. 4B and C). In addition, the PI4P production by PI4KB in the GUV model system was comparable with or without the 14-3-3 protein (Fig. 4B) as measured by the fluorescent PI4P biosensor CFP-SidC (Klima et al., 2017).

However, in cells PI4KB was reported to be activated by 14-3-3 proteins (Hausser et al., 2005, 2006). If 14-3-3 proteins do not activate PI4KB enzyme directly then a different mechanism must be in place. We speculated that 14-3-3 proteins could protect PI4KB from degradation. That would be, in fact, in good agreement with our structural analysis, which reveals that 14-3-3 proteins bind a disordered segment of PI4KB and thus can protect it from proteolytical degradation. This mode of action was already reported for 14-3-3 proteins previously (Cotelle et al., 2000; Dar et al., 2014; Dobson et al., 2011; Weiner and Kaiser, 1999). For instance, 14-3-3 proteins were shown to protect the FoxO3 transcription factor from degradation (Dobson et al., 2011) or for the Ctd2 (a substrate recognition adaptor of $CRL4^{Cdt2}$ E3 ubiquitin ligase complex) (Dar et al., 2014) and in plants it was shown that 14-3-3 proteins regulate global proteolytical cleavage of their diverse binding partners (Cotelle et al., 2000). We performed a protease degradation assay (Fig. 5) and we discovered that 14-3-3 proteins are able to protect phosphorylated PI4KB but not non-phosphorylated PI4KB from degradation by both chymotrypsin and Zymit (a commercial mixture with strong proteolytic activity) *in vitro*. It is tempting to speculate that 14-3-3 proteins act as molecular chaperones that stabilize PI4KB. However, this remains only a hypothesis until it can be confirmed *in vivo*.

3. Experimental procedures

3.1. Protein expression and purification

The recombinant proteins (PI4KB, 14-3-3, GFP-14-3-3, CFP-SidC, ACBD3, PKA) were expressed and purified using our standard methods (Hercik et al., 2017; Nemecek et al., 2013) that were modified for PI4KB as described previously (Burke et al., 2014; Mejdrova et al., 2015). Briefly the disordered N-terminal region 1-127 and a disordered loop 423-522 were deleted. These deletions do not significantly affect the enzymatic activity of the enzyme (Fowler et al., 2016). However, the disordered C-terminus (amino acids 800-816) is required for enzymatic activity and was deleted only for SAXS experiments. 14-3-3 proteins bind PI4KB phosphorylated at the residue S294. To produce phosphorylated PI4KB we adopted a widely used strategy where the sequence of the phosphorylation site is mutated to be recognized by the cAMP-dependent protein kinase (PKA) (Obsilova et al., 2008b). In this case, the introduction of a single point mutation (T292R) was sufficient. PI4KB was expressed as a fusion protein with His_{8x} –SUMO (SMT3 from *S. cerevisiae*) tag in *E. coli* BL21 Star. Cells were grown overnight in auto

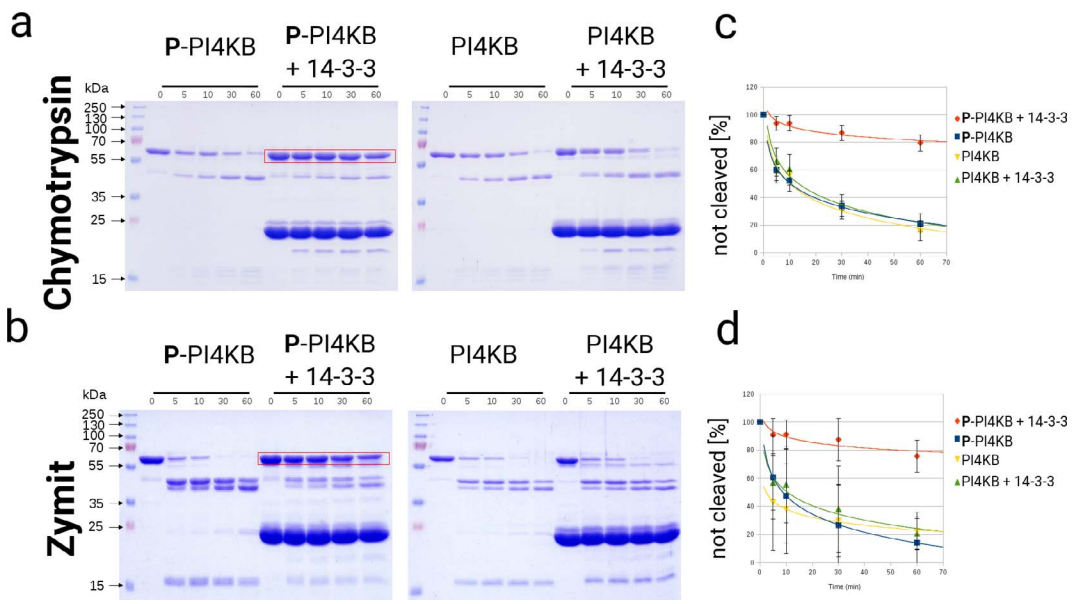

Fig. 5. Limited proteolysis assay was used to test whether binding of 14-3-3 to phosphorylated PI4KB (P-PI4KB) has a protective effect. PI4KB or P-PI4KB in the absence or presence of 14-3-3 was digested by chymotrypsin (A) or by Zymit (B) for 5, 10, 30 and 60 min. Undigested protein served as the zero-time point. The reactions were terminated by adding SDS-PAGE sample loading buffer and boiling 5 min before they were analyzed by SDS-PAGE. One representative picture is shown for each of the three independent experiments. Red rectangle marks highlight P-PI4KB protected from proteolytical degradation. The density of bands representing PI4KB from the individual experiments were quantified using ImageJ (Schindelin et al., 2015). The quantification of PI4KB degradation in the three independent experiments are shown for both chymotrypsin (C) and Zymit (D) in graphs with associated errors (s.d.).

induction media, harvested by centrifugation, resuspended in lysis buffer (50 mM Tris pH 8.0, 20 mM imidazole, 300 mM NaCl, 10% glycerol, and 3 mM β-mercaptoethanol) and lysed using EmulsiFlex C3. Subsequently, the lysate was cleared by centrifugation and the proteins were purified from the supernatant by affinity chromatography on a Ni-NTA resin (Machery-Nagel). Column. His_{8x} –SUMO was cleaved by SUMO protease (Ulp1 from *S. cerevisiae*) and PI4KB was then dialyzed to 20 mM Tris-HCl (pH 7.4), 150 mM NaCl, 3 mM β-mercaptoethanol. Optionally, recombinant PI4KB was phosphorylated by incubation with PKA (4 μg of PKA per 1 mg of PI4KB) for 2 h at 26 °C and then overnight at 4 °C in buffer containing 20 mM pH 7.4, 150 mM NaCl, 2 mM DTT, 300 μM ATP, 10 mM $MgCl_2$. PI4KB was further purified using anion-exchange chromatography on Mono Q 5/50GL (GE Healthcare) and size-exclusion chromatography on a Superdex 200 HiLoad 16/60 column (GE Healthcare) in SEC buffer (20 mM Tris pH 8.0, 200 mM NaCl, 3 mM β-mercaptoethanol). Phosphorylation was finally checked using mass spectroscopy and because we were unable to observe a peak of non-phosphorylated PI4KB we assumed ~100% efficiency of the phosphorylation reaction.

3.2. Analytical ultracentrifugation analysis

Sedimentation velocity (SV) experiments were performed at 20 °C and 42,000 rpm in a Beckman Coulter ProteomeLab XL-I analytical ultracentrifuge using standard protocols (Brown et al., 2008; Zhao et al., 2013a). All measurements were conducted in 20 mM Tris, pH 8.0, supplemented with 200 mM NaCl, 3 mM βME and collected with an absorbance (250 and 280 nm) or interference optical system. Proteins were measured at the concentration of 2–20 μM and mixed at different ratios. Protein partial specific volumes, solution density and viscosity were calculated in SEDNTERP (http://sednterp.unh.edu/). Data were analyzed in terms of a continuous c(s) distribution of Lamm equation solutions with the software SEDFIT (Schuck, 2000). Scan file time-stamps were corrected (Zhao et al., 2013b) and good fits were obtained with r.m.s.d. values corresponding to typical instrument noise values.

3.3. Microscale thermophoresis (MST)

The MST technology (Jerabek-Willemsen et al., 2014) was used to determine solution equilibrium binding constants between PI4KB (phosphorylated versus non-phosphorylated) and the fusion protein GFP-14-3-3ζ. All measurements were performed using Monolith NT.115 (NanoTemper Technologies GmbH). We used 100 nM GFP-14-3-3 ζ and PI4KB or phosphorylated PI4KB in the concentration range from 4.4 nM to 36 μM in binding buffer (20 mM Tris pH 8.0, 200 mM NaCl, 3 mM β-mercaptoethanol). Samples were loaded into capillaries NT.115 (standard treated) and the thermophoresis signals were measured at 22 °C with a light-emitting diode (LED) power of 20% and MST power of 50%. The changes in thermophoresis were analyzed with the Monolith NT Analysis Software and the data were visualized with the LibreOffice software package.

3.4. Crystallization and crystallographic analysis

For crystallization, 14-3-3ζ was mixed with PI4KB derived peptide 289-LKRTApSNPKV-298 (Eisenreichova et al., 2016) in a 1:1.4 M ratio. The crystals were obtained by mixing 300 nl protein solution with 300 nl well solution (0.1M MES pH6, 10% PEG 8000, 20% ethylene glycol) in a sitting drop. The crystals grew within three days, were flash-cooled in liquid nitrogen and analysed at the BESSY-II beamline 14.1 (Mueller et al., 2012). They belonged to the orthorhombic $P2_12_12_1$ space group and diffracted to 2.1 Å. Diffraction data were processed using XDSAPP (Krug et al., 2012) and the structure was solved by molecular replacement in Phaser (McCoy et al., 2007) using previously solved structure of 14-3-3 protein (PDB entry 1a4o) as a search model and subsequently refined in Phenix (Adams et al., 2010) and Coot (Debreczeni and Emsley, 2012) to R_{work} = 18.79% and R_{free} = 23.11% good stereochemistry as summarized in Table 1. The structure was deposited in the PDB databank (http://www.rcsb.org/pdb) under accession code: 5NAS.

3.5. Small angle X-ray scattering (SAXS) measurements

An equimolar mixture of phosphorylated PI4KB and 14-3-3ζ

(122 μM each) was passed through Superdex 200 10/300 GL column in SAXS buffer (20 mM Tris pH 8.0, 150 mM NaCl, 1 mM TCEP, 1% glycerol). The complex was subsequently concentrated to 1.17 mg/ml, 2.72 mg/ml and 3.97 mg/ml (concentration was determined by UV absorbance). Samples were analysed on the BioSAXS Beamline BM29 (ESRF Grenoble) and EMBL SAXS beamline P12 at the Petra III storage ring at DESY (Deutsches Elektronen-Synchrotron, Hamburg, Germany).

3.6. Molecular simulations and SAXS analysis of PI4KB:14-3-3 protein complex

To sample physical conformations of the PI4KB:14-3-3 protein complex in solution, we used a coarse-grained model introduced by Kim and Hummer (Kim and Hummer, 2008). Here, the crystallized PI4KB as well as the crystallized phosphopeptide-bound 14-3-3ζ dimer were treated as rigid bodies whereas the flexible loops and disordered segments within PI4KB were simulated as chains of amino-acid beads with appropriate bending, stretching and torsional potentials (Kim and Hummer, 2008). We performed eight independent Monte Carlo (MC) simulations of the PI4KB:14-3-3 protein complex with 2:2 stoichiometry. To enhance sampling and generate a pool of diverse structures for SAXS analysis, the replica exchange (RE) method was adopted with replicas at eight different temperatures ranging from 300 K to 500 K. Each of the REMC simulations was started from a different conformation of the PI4KB:14-3-3 complex, and involved $2.5{\cdot}10^6$ MC sweeps. The simulation structures were saved every 1000 MC sweeps. In this way we obtained 8*8 = 64 trajectories containing 2500 simulation structures each.

The resulting pool of structures was found to be very diverse: The simulation structures had the radius of gyration, R_g, ranging from 39 to 64 Å. Their maximum extension, D_{max}, was found to vary between 115 and 215 Å. The overall shapes of the structures could be described by a distortion parameter, w (Rozycki et al., 2015). Elongated cigar-like shapes are characterized by substantial positive values of w, globular shapes correspond to $w \approx 0$, and pancake-like shapes yield substantial negative values of w. The distortion parameter of the simulated conformations of the PI4KB:14-3-3 protein complex was found to be in the range between -0.1 and 0.5.

The scattering intensity profile was computed for each of the simulation structures individually using the coarse-grained algorithm that was co-developed with the EROS method (Rozycki et al., 2011). In these calculations, the electron density of solvent was taken to be equal to 0.334 e/Å^3, and the electron density contrast of the hydration shell was assumed to be 0.03 e/Å^3. These quantities are the default values of parameters of CRYSOL (Svergun et al., 1995). The discrepancy between the experimental SAXS data, $I_{exp}(q)$, and the scattering intensity profile of the k-th simulation structure, $I_k(q)$, was quantified by

$$\chi_k^2 = \sum_{i=1}^{N_q} \frac{(I_{exp}(q_i) - aI_k(q_i) + b)^2}{\sigma^2(q_i)}$$

Here, index k labels the simulation structures, N_q is the number of data points, $\sigma(q)$ is the statistical error of intensity $I_{exp}(q)$, whereas a and b are fitting parameters obtained from conditions $\partial\chi^2/\partial a = 0$ and $\partial\chi^2/\partial b = 0$. The parameter a sets the intensity scale and the parameter $b \ll I_{exp}$ (q = 0) is a background correction (Francis et al., 2011).

Out of the pool of 64*2500 = 160,000 simulation structures, we selected 20 models with the smallest values of χ^2, which were found to be within the range from 1.54 to 1.66. To make a structural comparison of the top 20 models, we sorted them into groups, or clusters, on the basis of the relative positions of the two PI4KB monomers. We used the QT-clustering method with DRMS as metric (Rozycki et al., 2011). We obtained one major cluster and two or three minor clusters, depending on the cutoff on DRMS. For the DRMS cutoff of 6 Å, the major cluster contains 12 models, and the two minor clusters contain 5 and 3 models, respectively.

3.7. Pull-down assays

Pull-down experiments were performed using purified recombinant proteins. Fusion proteins His_{8x}-SUMO-PI4KB (8 μM) or phosphorylated His_{8x}-SUMO-PI4KB(8 μM) were immobilized on Ni-NTA agarose beads, washed with wash buffer (50 mM Tris pH 8.0, 150 mM NaCl, 20 mM imidazole, 3 mM β-mercaptoethanol) and then incubated with 8 μM 14-3-3. The beads were washed two times with wash buffer and bound proteins were eluted with wash buffer supplemented with 300 mM imidazole. Eluted protein samples were analyzed by SDS-PAGE.

3.8. Lipid kinase assay

The enzymatic activity of PI4KB was determined using the ADP-GloTM Kinase Assay (Promega) as described previously (Tai et al., 2011). Reactions were carried out in a total volume of 5 μl and contained 50 μM PI, 2 μM PI4KB or phosphorylated PI4KB, and a concentration series of 14-3-3 ranging from 0 to 20 μM. The reaction was started by adding ATP to final concentration 100 μM. All the components were diluted in kinase buffer (20 mM Tris pH 7.5, 5 mM $MgCl_2$; 0,2% Triton-X, 0.1 mg/ml BSA, 2 mM DTT). The reaction was carried out for 60 min at 25 °C and the amount of hydrolyzed ATP was measured according to the manufacturer's instructions using spectrophotometer TECAN infinite M 1000.

3.9. Limited proteolysis assay

PI4KB or phosphorylated PI4KB in the absence or presence of 14-3-3 was digested by chymotrypsin (0.25 μg/ml in 60 mM Tris pH 7.8, 150 mM NaCl, 10 mM $CaCl_2$) or by Zymit (100 000 times diluted commercial enzyme mixture in 50 mM Tris pH 8, 150 mM NaCl) for 5, 10, 30 and 60 min. Undigested protein served as the zero-time point. The reactions were terminated by adding SDS-PAGE sample loading buffer and boiling for 5 min. The results were analyzed by SDS-PAGE.

3.10. Giant unilamellar vesicles (GUVs) preparation and imaging

GUVs were prepared as before (Boura et al., 2012a), briefly, chloroform lipid mixture containing 54.99 mol% of POPC, 10 mol% POPS, 10 mol% PI, 20 mol% cholesterol, 5 mol% DGS-NTA(Ni) and 0.01 mol% ATTO647NDOPE (all Avanti Polar Lipids) was prepared at overall lipid concentration 5 μg/μL. 10 μL of the lipid mixture was spread on two ITO coated glass electrodes each. The electrodes were dried under vacuum overnight and then parallel assembled into a home made Teflon chamber containing 5 mL of 600 mM sucrose solution. For the electroformation, 10 kHz, harmonically oscillating voltage of 1 V peak value was applied to the electrodes for 1 h at 60 °C. For imaging, BSA-coated 4-chamber glass bottom dish (In Vitro Scientific) were used. 100 μL of GUVs mixed with 100 μL isosmotic buffer (25 mM Tris pH 8, 10 mM MgCl2, 20 mM Imidazole, 261.5 mM NaCl, 2 mM βME) containing proteins of interest and ATP, so that the final concentrations were: 600 nM (ACBD3, PI4KB), 20 μM (14-3-3ζ), 250 nM (SidC-CFP), and 1 mM (ATP).

The images of GUVs were acquired on LSM 710 confocal microscope (Zeiss, Jena, Germany) using 40×/1.2 water objective. The images were taken line-sequentially in two tracks: CFP and ATTO647N (excitation/emission wavelengths: 405 nm/454–490 nm, and 625 nm/645–759 nm, respectively), and Alexa488 (488 nm/499–595 nm).

Acknowledgements

We are grateful to the BioSAXS Beamline BM29 (ESRF Grenoble) and EMBL SAXS beamline P12 (Petra III DESY, Hamburg) for allocation of experimental beamtime. The project was supported by Czech Science Foundation grant number 17-05200S (to EB) and by the National Science Centre, Poland, grant number 2016/21/B/NZ1/00006 (to BR).

The Academy of Sciences of Czech Republic support (RVO: 61388963) is also acknowledged.

Conflict of interests

The authors declare no conflict of interests.

Author contributions

DC performed most of the experiments, AE contributed the crystallographic analysis, BR performed MD simulations and analyzed SAXS data, LR performed AUC analysis, JH performed GUV experiments, MK performed MST experiments, EB designed the study, supervised the project and wrote the manuscript. All authors commented on the manuscript and prepared figures from their data.

References

Adams, P.D., Afonine, P.V., Bunkoczi, G., Chen, V.B., Davis, I.W., Echols, N., Headd, J.J., Hung, L.W., Kapral, G.J., Grosse-Kunstleve, R.W., McCoy, A.J., Moriarty, N.W., Oeffner, R., Read, R.J., Richardson, D.C., Richardson, J.S., Terwilliger, T.C., Zwart, P.H., 2010. PHENIX: a comprehensive Python-based system for macromolecular structure solution. Acta Crystallogr., Sect D: Biol. Crystallogr. 66, 213–221.

Aghazadeh, Y., Papadopoulos, V., 2016. The role of the 14-3-3 protein family in health, disease, and drug development. Drug Discovery Today 21, 278–287.

Altan-Bonnet, N., Balla, T., 2012. Phosphatidylinositol 4-kinases: hostages harnessed to build panviral replication platforms. Trends Biochem. Sci. 37, 293–302.

Balla, T., 2013. Phosphoinositides: tiny lipids with giant impact on cell regulation. Physiol. Rev. 93, 1019–1137.

Baumlova, A., Gregor, J., Boura, E., 2016. The structural basis for calcium inhibition of lipid kinase PI4K IIalpha and comparison with the apo state. Physiol. Res./Academia Scientiarum Bohemoslovaca 65, 987–993.

Baumlova, A., Chalupska, D., Rozycki, B., Jovic, M., Wisniewski, E., Klima, M., Dubankova, A., Kloer, D.P., Nencka, R., Balla, T., Boura, E., 2014. The crystal structure of the phosphatidylinositol 4-kinase IIalpha. EMBO Rep. 15, 1085–1092.

Berger, K.L., Cooper, J.D., Heaton, N.S., Yoon, R., Oakland, T.E., Jordan, T.X., Mateu, G., Grakoui, A., Randall, G., 2009. Roles for endocytic trafficking and phosphatidylinositol 4-kinase III alpha in hepatitis C virus replication. Proc. Natl. Acad. Sci. U.S.A. 106, 7577–7582.

Boura, E., Hurley, J.H., 2012. Structural basis for membrane targeting by the MVB12-associated beta-prism domain of the human ESCRT-I MVB12 subunit. Proc. Natl. Acad. Sci. U.S.A. 109, 1901–1906.

Boura, E., Nencka, R., 2015. Phosphatidylinositol 4-kinases: function, structure, and inhibition. Experim. Cell Res. 337, 136–145.

Boura, E., Rezabkova, L., Brynda, J., Obsilova, V., Obsil, T., 2010. Structure of the human FOXO4-DBD-DNA complex at 1.9 A resolution reveals new details of FOXO binding to the DNA. Acta Crystallogr., Sect D: Biol. Crystallogr. 66, 1351–1357.

Boura, E., Ivanov, V., Carlson, L.A., Mizuuchi, K., Hurley, J.H., 2012a. Endosomal sorting complex required for transport (ESCRT) complexes induce phase-separated microdomains in supported lipid bilayers. J. Biol. Chem. 287, 28144–28151.

Boura, E., Rozycki, B., Herrick, D.Z., Chung, H.S., Vecer, J., Eaton, W.A., Cafiso, D.S., Hummer, G., Hurley, J.H., 2011. Solution structure of the ESCRT-I complex by small-angle X-ray scattering, EPR, and FRET spectroscopy. Proc. Natl. Acad. Sci. U.S.A. 108, 9437–9442.

Boura, E., Rozycki, B., Chung, H.S., Herrick, D.Z., Canagarajah, B., Cafiso, D.S., Eaton, W.A., Hummer, G., Hurley, J.H., 2012b. Solution structure of the ESCRT-I and -II supercomplex: implications for membrane budding and scission. Structure 20, 874–886.

Brown, P.H., Balbo, A., Schuck, P., 2008. Characterizing protein-protein interactions by sedimentation velocity analytical ultracentrifugation. Current protocols in immunology. John, E. Coligan, et al. (Eds.), Chapter 18, Unit 18 15.

Burke, J.E., Inglis, A.J., Perisic, O., Masson, G.R., McLaughlin, S.H., Rutaganira, F., Shokat, K.M., Williams, R.L., 2014. Structures of PI4KIIIbeta complexes show simultaneous recruitment of Rab11 and its effectors. Science 344, 1035–1038.

Clayton, E.L., Minogue, S., Waugh, M.G., 2013. Mammalian phosphatidylinositol 4-kinases as modulators of membrane trafficking and lipid signaling networks. Prog. Lipid Res. 52, 294–304.

Cotelle, V., Meek, S.E.M., Provan, F., Milne, F.C., Morrice, N., MacKintosh, C., 2000. 14-3-3s regulate global cleavage of their diverse binding partners in sugar-starved Arabidopsis cells. EMBO J. 19, 2869–2876.

Dar, A., Wu, D., Lee, N., Shibata, E., Dutta, A., 2014. 14-3-3 proteins play a role in the cell cycle by shielding cdt2 from ubiquitin-mediated degradation. Mol. Cell. Biol. 34, 4049–4061.

de Boer, A.H., van Kleeff, P.J.M., Gao, J., 2013. Plant 14-3-3 proteins as spiders in a web of phosphorylation. Protoplasma 250, 425–440.

Debreczeni, J.E., Emsley, P., 2012. Handling ligands with Coot. Acta Crystallogr., Sect D: Biol. Crystallogr. 68, 425–430.

Dent, P., Jelinek, T., Morrison, D.K., Weber, M.J., Sturgill, T.W., 1995. Reversal of Raf-1 activation by purified and membrane-associated protein phosphatases (Vol 268, Pg 1902, 1995). Science 269, 1657.

Dobson, M., Ramakrishnan, G., Ma, S., Kaplun, L., Balan, V., Fridman, R., Tzivion, G., 2011. Bimodal regulation of FoxO3 by AKT and 14-3-3. Biochim. Biophys. Acta 1813, 1453–1464.

Dornan, G.L., McPhail, J.A., Burke, J.E., 2016. Type III phosphatidylinositol 4 kinases: structure, function, regulation, signalling and involvement in disease. Biochem. Soc. Trans. 44, 260–266.

Eisenreichova, A., Klima, M., Boura, E., 2016. Crystal structures of a yeast 14-3-3 protein from Lachancea thermotolerans in the unliganded form and bound to a human lipid kinase PI4KB-derived peptide reveal high evolutionary conservation. Acta Crystallogr. F Struct. Biol. Commun. 72, 799–803.

Fowler, M.L., McPhail, J.A., Jenkins, M.L., Masson, G.R., Rutaganira, F.U., Shokat, K.M., Williams, R.L., Burke, J.E., 2016. Using hydrogen deuterium exchange mass spectrometry to engineer optimized constructs for crystallization of protein complexes: Case study of PI4KIIIbeta with Rab11. Protein science: a publication of the Protein Society.

Francis, D.M., Rozycki, B., Tortajada, A., Hummer, G., Peti, W., Page, R., 2011. Resting and active states of the ERK2:HePTP complex. J. Am. Chem. Soc. 133, 17138–17141.

Ganguly, S., Gastel, J.A., Weller, J.L., Schwartz, C., Jaffe, H., Namboodiri, M.A., Coon, S.L., Hickman, A.B., Rollag, M., Obsil, T., Beauverger, P., Ferry, G., Boutin, J.A., Klein, D.C., 2001. Role of a pineal cAMP-operated arylalkylamine N-acetyltransferase/14-3-3-binding switch in melatonin synthesis. Proc. Natl. Acad. Sci. U.S.A. 98, 8083–8088.

Greninger, A.L., Knudsen, G.M., Betegon, M., Burlingame, A.L., Derisi, J.L., 2012. The 3A protein from multiple picornaviruses utilizes the golgi adaptor protein ACBD3 to recruit PI4KIIIbeta. J. Virol. 86, 3605–3616.

Hausser, A., Storz, P., Martens, S., Link, G., Toker, A., Pfizenmaier, K., 2005. Protein kinase D regulates vesicular transport by phosphorylating and activating phosphatidylinositol-4 kinase IIIbeta at the Golgi complex. Nat. Cell Biol. 7, 880–886.

Hausser, A., Link, G., Hoene, M., Russo, C., Selchow, O., Pfizenmaier, K., 2006. Phospho-specific binding of 14-3-3 proteins to phosphatidylinositol 4-kinase III beta protects from dephosphorylation and stabilizes lipid kinase activity. J. Cell Sci. 119, 3613–3621.

Hercik, K., Kozak, J., Sala, M., Dejmek, M., Hrebabecky, H., Zbornikova, E., Smola, M., Ruzek, D., Nencka, R., Boura, E., 2017. Adenosine triphosphate analogs can efficiently inhibit the Zika virus RNA-dependent RNA polymerase. Antiviral Res. 137, 131–133.

Humpolickova, J., Mejdrova, I., Matousova, M., Nencka, R., Boura, E., 2017. Fluorescent inhibitors as tools to characterize enzymes: case study of the lipid kinase phosphatidylinositol 4-kinase IIIbeta (PI4KB). J. Med. Chem. 60, 119–127.

Jerabek-Willemsen, M., Andre, T., Wanner, R., Roth, H.M., Duhr, S., Baaske, P., Breitsprecher, D., 2014. MicroScale thermophoresis: interaction analysis and beyond. J. Mol. Struct. 1077, 101–113.

Jovic, M., Kean, M.J., Szentpetery, Z., Polevoy, G., Gingras, A.C., Brill, J.A., Balla, T., 2012. Two phosphatidylinositol 4-kinases control lysosomal delivery of the Gaucher disease enzyme, beta-glucocerebrosidase. Mol. Biol. Cell 23, 1533–1545.

Jovic, M., Kean, M.J., Dubankova, A., Boura, E., Gingras, A.C., Brill, J.A., Balla, T., 2014. Endosomal sorting of VAMP3 is regulated by PI4K2A. J. Cell Sci. 127, 3745–3756.

Kacirova, M., Kosek, D., Kadek, A., Man, P., Vecer, J., Herman, P., Obsilova, V., Obsil, T., 2015. Structural characterization of phosducin and its complex with the 14-3-3 protein. J. Biol. Chem. 290, 16246–16260.

Kim, Y.C., Hummer, G., 2008. Coarse-grained models for simulations of multiprotein complexes: application to ubiquitin binding. J. Mol. Biol. 375, 1416–1433.

Klima, M., Baumlova, A., Chalupska, D., Hrebabecky, H., Dejmek, M., Nencka, R., Boura, E., 2015. The high-resolution crystal structure of phosphatidylinositol 4-kinase IIbeta and the crystal structure of phosphatidylinositol 4-kinase IIalpha containing a nucleoside analogue provide a structural basis for isoform-specific inhibitor design. Acta Crystallogr., Sect D: Biol. Crystallogr. 71, 1555–1563.

Klima, M., Chalupska, D., Rozycki, B., Humpolickova, J., Rezabkova, L., Silhan, J., Baumlova, A., Dubankova, A., Boura, E., 2017. Kobuviral non-structural 3A proteins act as molecular harnesses to hijack the host ACBD3 protein. Structure 25, 219–230.

Klima, M., Toth, D.J., Hexnerova, R., Baumlova, A., Chalupska, D., Tykvart, J., Rezabkova, L., Sengupta, N., Man, P., Dubankova, A., Humpolickova, J., Nencka, R., Veverka, V., Balla, T., Boura, E., 2016. Structural insights and in vitro reconstitution of membrane targeting and activation of human PI4KB by the ACBD3 protein. Sci. Rep. 6, 23641.

Krug, M., Weiss, M.S., Heinemann, U., Mueller, U., 2012. XDSAPP: a graphical user interface for the convenient processing of diffraction data using XDS. J. Appl. Crystallogr. 45, 568–572.

Lambeck, I.C., Fischer-Schrader, K., Niks, D., Roeper, J., Chi, J.C., Hille, R., Schwarz, G., 2012. Molecular mechanism of 14-3-3 protein-mediated inhibition of plant nitrate reductase. J. Biol. Chem. 287, 4562–4571.

Liu, D., Bienkowska, J., Petosa, C., Collier, R.J., Fu, H., Liddington, R., 1995. Crystal structure of the zeta isoform of the 14-3-3 protein. Nature 376, 191–194.

McCoy, A.J., Grosse-Kunstleve, R.W., Adams, P.D., Winn, M.D., Storoni, L.C., Read, R.J., 2007. Phaser crystallographic software. J. Appl. Crystallogr. 40, 658–674.

McPhail, J.A., Ottosen, E.H., Jenkins, M.L., Burke, J.E., 2017. The molecular basis of aichi virus 3A protein activation of phosphatidylinositol 4 kinase IIIbeta, PI4KB, through ACBD3. Structure 25, 121–131.

Mejdrova, I., Chalupska, D., Kogler, M., Sala, M., Plackova, P., Baumlova, A., Hrebabecky, H., Prochazkova, E., Dejmek, M., Guillon, R., Strunin, D., Weber, J., Lee, G., Birkus, G., Mertlikova-Kaiserova, H., Boura, E., Nencka, R., 2015. Highly Selective phosphatidylinositol 4-kinase IIIbeta inhibitors and structural insight into their mode of action. J. Med. Chem. 58, 3767–3793.

Mejdrova, I., Chalupska, D., Plackova, P., Muller, C., Sala, M., Klima, M., Baumlova, A., Hrebabecky, H., Prochazkova, E., Dejmek, M., Strunin, D., Weber, J., Lee, G., Matousova, M., Mertlikova-Kaiserova, H., Ziebuhr, J., Birkus, G., Boura, E., Nencka,

R., 2017. Rational design of novel highly potent and selective phosphatidylinositol 4-kinase IIIbeta (PI4KB) inhibitors as broad-spectrum antiviral agents and tools for chemical biology. J. Med. Chem. 60, 100–118.
Morrison, D.K., 2009. The 14-3-3 proteins: integrators of diverse signaling cues that impact cell fate and cancer development. Trends Cell Biol. 19, 16–23.
Mueller, U., Darowski, N., Fuchs, M.R., Forster, R., Hellmig, M., Paithankar, K.S., Puhringer, S., Steffien, M., Zocher, G., Weiss, M.S., 2012. Facilities for macromolecular crystallography at the Helmholtz-Zentrum Berlin. J. Synchrotron Radiat. 19, 442–449.
Nemecek, D., Boura, E., Wu, W., Cheng, N., Plevka, P., Qiao, J., Mindich, L., Heymann, J.B., Hurley, J.H., Steven, A.C., 2013. Subunit folds and maturation pathway of a dsRNA virus capsid. Structure 21, 1374–1383.
Obsilova, V., Silhan, J., Boura, E., Teisinger, J., Obsil, T., 2008a. 14-3-3 proteins: a family of versatile molecular regulators. Physiol. Res./Academia Scientiarum Bohemoslovaca 57 (Suppl 3), S11–21.
Obsilova, V., Kopecka, M., Kosek, D., Kacirova, M., Kylarova, S., Rezabkova, L., Obsil, T., 2014. Mechanisms of the 14-3-3 protein function: regulation of protein function through conformational modulation. Physiol. Res./Academia Scientiarum Bohemoslovaca 63 (Suppl 1), S155–164.
Obsilova, V., Vecer, J., Herman, P., Pabianova, A., Sulc, M., Teisinger, J., Boura, E., Obsil, T., 2005. 14-3-3 Protein interacts with nuclear localization sequence of forkhead transcription factor FoxO4. Biochemistry 44, 11608–11617.
Obsilova, V., Nedbalkova, E., Silhan, J., Boura, E., Herman, P., Vecer, J., Sulc, M., Teisinger, J., Dyda, F., Obsil, T., 2008b. The 14-3-3 protein affects the conformation of the regulatory domain of human tyrosine hydroxylase. Biochemistry 47, 1768–1777.
Rezabkova, L., Man, P., Novak, P., Herman, P., Vecer, J., Obsilova, V., Obsil, T., 2011. Structural basis for the 14-3-3 protein-dependent inhibition of the regulator of G protein signaling 3 (RGS3) function. J. Biol. Chem. 286, 43527–43536.
Rezabkova, L., Boura, E., Herman, P., Vecer, J., Bourova, L., Sulc, M., Svoboda, P., Obsilova, V., Obsil, T., 2010. 14-3-3 protein interacts with and affects the structure of RGS domain of regulator of G protein signaling 3 (RGS3). J. Struct. Biol. 170, 451–461.
Rozycki, B., Boura, E., 2014. Large, dynamic, multi-protein complexes: a challenge for structural biology. Journal of physics. Condensed matter: an Institute of Physics journal 26, 463103.
Rozycki, B., Kim, Y.C., Hummer, G., 2011. SAXS ensemble refinement of ESCRT-III CHMP3 conformational transitions. Structure 19, 109–116.
Rozycki, B., Cieplak, M., Czjzek, M., 2015. Large conformational fluctuations of the multi-domain xylanase Z of Clostridium thermocellum. J. Struct. Biol. 191, 68–75.
Rozycki, B., Boura, E., Hurley, J.H., Hummer, G., 2012. Membrane-elasticity model of Coatless vesicle budding induced by ESCRT complexes. PLoS Comput. Biol. 8, e1002736.
Rutaganira, F.U., Fowler, M.L., McPhail, J.A., Gelman, M.A., Nguyen, K., Xiong, A., Dornan, G.L., Tavshanjian, B., Glenn, J.S., Shokat, K.M., Burke, J.E., 2016. Design and structural characterization of potent and selective inhibitors of phosphatidylinositol 4 kinase IIIbeta. J. Med. Chem. 59, 1830–1839.
Sala, M., Kogler, M., Plackova, P., Mejdrova, I., Hrebabecky, H., Prochazkova, E., Strunin, D., Lee, G., Birkus, G., Weber, J., Mertlikova-Kaiserova, H., Nencka, R., 2016. Purine analogs as phosphatidylinositol 4-kinase IIIbeta inhibitors. Bioorg. Med. Chem. Lett. 26, 2706–2712.
Sasaki, J., Ishikawa, K., Arita, M., Taniguchi, K., 2012. ACBD3-mediated recruitment of PI4KB to picornavirus RNA replication sites. EMBO J. 31, 754–766.
Schindelin, J., Rueden, C.T., Hiner, M.C., Eliceiri, K.W., 2015. The ImageJ ecosystem: an open platform for biomedical image analysis. Mol. Reprod. Dev. 82, 518–529.
Schuck, P., 2000. Size-distribution analysis of macromolecules by sedimentation velocity ultracentrifugation and lamm equation modeling. Biophys. J. 78, 1606–1619.
Simons, J.P., Al-Shawi, R., Minogue, S., Waugh, M.G., Wiedemann, C., Evangelou, S., Loesch, A., Sihra, T.S., King, R., Warner, T.T., Hsuan, J.J., 2009. Loss of phosphatidylinositol 4-kinase 2alpha activity causes late onset degeneration of spinal cord axons. Proc. Natl. Acad. Sci. U.S.A. 106, 11535–11539.
Svergun, D., Barberato, C., Koch, M.H.J., 1995. CRYSOL – a program to evaluate x-ray solution scattering of biological macromolecules from atomic coordinates. J. Appl. Crystallogr. 28, 768–773.
Tai, A.W., Bojjireddy, N., Balla, T., 2011. A homogeneous and nonisotopic assay for phosphatidylinositol 4-kinases. Anal. Biochem. 417, 97–102.
Tan, J., Brill, J.A., 2014. Cinderella story: PI4P goes from precursor to key signaling molecule. Crit. Rev. Biochem. Mol. Biol. 49, 33–58.
Thorson, J.A., Yu, L.W., Hsu, A.L., Shih, N.Y., Graves, P.R., Tanner, J.W., Allen, P.M., Piwnica-Worms, H., Shaw, A.S., 1998. 14-3-3 proteins are required for maintenance of Raf-1 phosphorylation and kinase activity. Mol. Cell. Biol. 18, 5229–5238.
Uhart, M., Bustos, D.M., 2014. Protein intrinsic disorder and network connectivity. The case of 14-3-3 proteins. Front. Genet. 5, 10.
van der Schaar, H.M., Leyssen, P., Thibaut, H.J., de Palma, A., van der Linden, L., Lanke, K.H., Lacroix, C., Verbeken, E., Conrath, K., Macleod, A.M., Mitchell, D.R., Palmer, N.J., van de Poel, H., Andrews, M., Neyts, J., van Kuppeveld, F.J., 2013. A novel, broad-spectrum inhibitor of enterovirus replication that targets host cell factor phosphatidylinositol 4-kinase IIIbeta. Antimicrob. Agents Chemother. 57, 4971–4981.
Waugh, M.G., 2012. Phosphatidylinositol 4-kinases, phosphatidylinositol 4-phosphate and cancer. Cancer Lett. 325, 125–131.
Waugh, M.G., 2015. PIPs in neurological diseases. Biochim. Biophys. Acta 1851, 1066–1082.
Weiner, H., Kaiser, W.M., 1999. 14-3-3 proteins control proteolysis of nitrate reductase in spinach leaves. FEBS Lett. 455, 75–78.
Zhao, H., Brautigam, C.A., Ghirlando, R., Schuck, P., 2013a. Overview of current methods in sedimentation velocity and sedimentation equilibrium analytical ultracentrifugation. Current protocols in protein science/editorial board. John, E. Coligan, et al. (Eds.), Chapter 20, Unit20 12.
Zhao, H., Ghirlando, R., Piszczek, G., Curth, U., Brautigam, C.A., Schuck, P., 2013b. Recorded scan times can limit the accuracy of sedimentation coefficients in analytical ultracentrifugation. Anal. Biochem. 437, 104–108.